Chin-Teng Lin, Te-Cheng Chiu, Yu-Kai Wang, Chun-Hsiang Chuang, Klaus Gramann

Granger causal connectivity dissociates navigation networks that subserve allocentric and egocentric path integration

Granger Causal Connectivity Dissociates Navigation Networks that Subserve Allocentric and Egocentric Path Integration

Chin-Teng Lin [1], Te-Cheng Chiu[2], Yu-Kai Wang[1],
Chun-Hsiang Chuang[1] and Klaus Gramann[3,4]

[1]Centre for Artificial Intelligence, Faculty of Engineering and Information Technology, University of Technology Sydney, Australia;
[2]Brain Research Center, National Chiao-Tung University, Hsinchu, Taiwan;
[3]Biological Psychology and Neuroergonomics, Technische Universitaet Berlin;
[4]Center for Advanced Neurological Engineering, University of California, San Diego, USA

DOI: 10. 1016/j.brainres.2017.11.016

Abstract

Studies on spatial navigation demonstrate a significant role of the retrosplenial complex (RSC) in the transformation of egocentric and allocentric information into complementary spatial reference frames (SRFs). The tight anatomical connections of the RSC with a wide range of other cortical regions processing spatial information support its vital role within the human navigation network. To better understand how different areas of the navigational network interact, we investigated the dynamic causal interactions of brain regions involved in solving a virtual navigation task. EEG signals were decomposed by independent component analysis (ICA) and subsequently examined for information flow between clusters of independent components (ICs) using direct short-time directed transfer function (sdDTF). The results revealed information flow between the anterior cingulate cortex and the left prefrontal cortex in the theta (4–7 Hz) frequency band and between the prefrontal, motor, parietal, and occipital cortices as well as the RSC in the alpha (8–13 Hz) frequency band. When

participants preference to use distinct reference frames (egocentric vs. allocentric) during navigation was considered, a dominant occipito-parieto–RSC network was identified in allocentric navigators. These results are in line with the assumption that the RSC, parietal, and occipital cortices are involved in transforming egocentric visual spatial information into an allocentric reference frame. Moreover, the RSC demonstrated the strongest causal flow during changes in orientation, suggesting that this structure directly provides information on heading changes in humans.

Keywords: spatial navigation, allocentric, egocentric, retrosplenial complex, brain connectivity

1. Introduction

Successful navigation in well-known and unknown environments requires simultaneous processing and integration of spatial information based on allocentric and egocentric spatial reference frames (SRFs) [Klatzky, 1998]. Reference frames are a means to represent spatial information based on egocentric or allocentric coordinate systems. An allocentric representational system is centered on aspects of the environment and represents the location of entities in space with respect to allothetic information like cardinal directions. In contrast, an egocentric representational system is centered on aspects of the navigator's physical structure and thus varies with changes in orientation of the navigator. Importantly, successful navigation requires integration of spatial

information from both egocentric and allocentric representations to allow goal-directed action in the environment (Gramann, 2013).

The computation, integration, and exchange of spatial information based different SRFs involves a network of brain structures including the medial temporal cortex, the cingulate gyrus, the frontal, parietal, and occipital cortices, as well as the retrosplenial complex (RSC) [Hartley et al., 2003; Maguire et al., 1998; Whitlock et al., 2008]. Imaging studies investigating the neural structures underlying egocentric and allocentric spatial navigation have revealed that the parietal cortex subserves the computation of egocentric SRFs by integrating self-motion cues from the kinesthetic, vestibular, and visual systems [Zaehle et al., 2007; Committeri et al., 2004; Cohen and Andersen, 2002]. In contrast, the use of an allocentric SRF mainly engages medial temporal brain structures [Doeller et al., 2010; Ekstrom et al., 2003; Howard et al., 2014; Jacobs et al., 2013; Maguire et al., 1998; Wolbers and Büchel, 2005]. Moreover, the RSC has been found to play important roles in computing and maintaining allocentric spatial representations and in transforming spatial information between egocentric and allocentric reference frames [Byrne et al., 2007; Dhindsa et al., 2014; Vann et al., 2009; Zhang et al., 2012].

Many of these brain areas are simultaneously active during navigation tasks, and coupling of functionally specialized brain regions appears to be necessary for successful navigation [Ekstrom et al., 2014]. Recent EEG studies have reported high coherence of the alpha and theta frequency bands in a large-scale cortical network recruited during spatial navigation [Li et al., 2009; Ramos-Loyo and

Sanchez-Loyo, 2011]. Connectivity across various brain areas with modulations in the theta and alpha frequency ranges may support the synchronization of large-scale cortical interactions [Palva and Palva, 2011; Sauseng et al., 2005] and is one of the essential neuronal mechanisms for higher cognitive functions [Siegel et al., 2012]. However, investigations describing the flow of information within these cortical networks with high temporal resolution are scarce, and the architecture of the spatial navigation network is not well understood.

To further our understanding of connectivity in the navigation network, we used high-density EEG and Granger causality analysis to investigate which brain regions are causally connected while participants updated their position and orientation during navigation. Previous studies using path integration paradigms showed that the individual preference to use either an egocentric or an allocentric reference frame is stable for individuals [Gramann et al., 2005], is based on higher cognitive functions [Gramann et al., 2009], depends on core areas of the navigation network [Gramann et al., 2006; Gramann et al., 2010; Seubert et al., 2008], and can be reliably observed in different populations [Gramann et al., 2012; Goeke et al., 2013; 2015]. Previous studies also demonstrated navigation-related modulations of distinct frequency bands that were dependent on the reference frame proclivity of participants [Chiu et al., 2012; Gramann et al., 2010; Lin et al., 2015; Plank et al., 2010]. To further investigate the information flow in the human navigation network and to understand how information flow differs between egocentric and allocentric navigators, we analyzed granger causal information flow in EEG data recorded during a virtual path integration task.

2. Results

For allocentric and egocentric participants, the behavioral performance including homing angle and homing position were reported. The analysis of direct information transfer between clusters of ICs revealed event related causality (ERC) in the time–frequency distribution between several cortical regions. Widespread brain regions were involved in path integration, revealing directed ERC between the anterior cingulate cortex (ACC), the RSC, and the lateral prefrontal, motor, parietal, and occipital cortices for all participants. The causal information flows were significantly increased in distinct frequency band including delta (below 3.5 Hz), theta (4–7 Hz), alpha (8–13 Hz), and beta (14–30 Hz).

2.1 Behavioral performance

The mean homing responses are displayed in Figure 1 for both allocentric and egocentric indicated as dotted and straight line, respectively. In Figure 1A, the result of homing response indicating that using an egocentric SRF indicated opposite homing directions as compared to homing responses of allocentric, using an allocentric SRF ($p < 0.01$). The homing responses for allocentric and egocentric consistently differed in each path configuration supported the hypothesis that both strategy groups used a distinct reference frame for their homing responses for path integration in the virtual navigation environment. The homing performance also shows the significant differences in homing error for allocentric and egocentric participants in Figure 1B ($p < 0.01$). In Figure 1B, egocentric reveals

117 higher accuracy for low eccentric end positions (18.4°, 26.5°, and 33.6), in contract,
118 the allocentric were more accurate for higher eccentricities (above 45°).
119
120 ********** insert Figure 1 here **********
121
122 **2.2 Time–frequency distribution of causal information inflow**
123 Figure 2 displays the average dynamic causal relationships between selected
124 anterior brain regions during path integration as compared to the baseline
125 condition for egocentric and allocentric participants (please see supplementary
126 Figure 1 for connectivity pattern between all clusters). As shown in Figure. 2,
127 significant ERC increases were observed between a cluster with its centroid
128 located in or near the ACC and clusters with their centroids located in or near the
129 left and right prefrontal areas (bootstrapping, false discovery rate (FDR)-adjusted
130 $p < 0.05$). The ERC flow between these areas was significant for the theta, the alpha,
131 and the beta frequency band (bootstrapping, FDR-adjusted $p < 0.05$). The
132 sustained bidirectional ERC increase in the theta and alpha band between ACC and
133 left prefrontal cortex (ACC<->LPF) was observed for both egocentric and
134 allocentric participants while only egocentric navigators showed ERC increases in
135 the beta band around 20 Hz (ACC->LPF & ACC->RPF). The prefrontal cortex
136 further revealed sustained ERC decreases from the left motor to the left prefrontal
137 cortex (LM->LPF) for allocentric navigators only. Additional sustained ERC
138 increases between the prefrontal cortex and posterior cortex was observed (see
139 supplementary Figure 1), from the left parietal to the left prefrontal cortex (LP-

>LPF).

********** insert Figure 2 here **********

The time course of ERC demonstrated more pronounced information flow in the theta band between ACC and the left motor cortex (ACC<->LM) for egocentric participants during the stimulus turn (see Figure 2). Reciprocal ERC in the alpha band between right prefrontal and the right motor cortex (RPF<->RM) increased during the stimulus turn and the following straight segments. For allocentric navigators, in contrast, alpha ERC from the left prefrontal cortex to the left motor cortex (LPF->LM) was strongest during stimulus turns and part of straight segments before and after the turn (see Figure 2). Allocentric participants also showed reciprocal alpha ERC between the right prefrontal cortex and the right motor cortex (RPF<->RM) mainly during straight segments (see Figure 2).

Stronger ERC increases were revealed in more posterior brain regions including the motor, the parietal, and the occipital cortex as well as the RSC (see Figure 3). ERC increases in the alpha band were found between motor and parietal areas during the complete path most pronounced for egocentric participants. Significant reciprocal alpha ERCs between the left and right motor cortices (LM<->RM) was only found for egocentric participants while alpha ERCs between the left and right parietal cortices (LP<->RP) were more pronounced in allocentric participants (bootstrapping, FDR-adjusted $p < 0.05$). Both strategy groups demonstrated stronger intrahemispheric ERC, for example, reciprocal alpha ERC

between the parietal and motor cortices within the right and left hemisphere were more pronounced than between the hemispheres. The left parietal cortex showed more pronounced ERC with anterior regions such as the prefrontal and motor cortices, whereas the right parietal cortex showed stronger ERC with posterior regions such as the RSC and occipital cortex (see supplementary Figure 1). This difference in the ERC pattern was more pronounced for allocentric participants (bootstrapping, FDR-adjusted $p < 0.05$).

********** insert Figure 3 here **********

In or near the RSC, ERC flows from and to the parietal and occipital cortices comprised a wider frequency range, including the delta and alpha bands. Bidirectional ERC between the RSC and parietal cortex (RSC<->RP) in the alpha and delta frequency bands was found for both allocentric and egocentric participants, although more pronounced in allocentric navigators (bootstrapping, FDR-adjusted $p < 0.05$). In the allocentric group, the RSC revealed alpha ERC with the right parietal cortex (RSC->RP) before and during stimulus turns. The RSC received weaker alpha flow from the right parietal cortex (PR->RSC). It is important to note that information flow between the RSC and parietal cortex increased in the higher alpha band (from 10 Hz to 12 Hz) before stimulus turns, whereas it increased in the low alpha band during stimulus turns (see Figure 3).

Reciprocal ERC between the RSC and the occipital cortex (RSC<->Occ) in the alpha and delta frequency bands was found for both allocentric and egocentric

navigators. Egocentric participants demonstrated reciprocal delta ERC during straight segments, before and after stimulus turns, and alpha ERC during stimulus turns. Allocentric participants demonstrated sustained, reciprocal delta and alpha ERC throughout the task. In addition, strategy-specific bidirectional alpha transfer between the RSC and the right motor cortex (RSC<->RM) was found only for egocentric navigators (see Figure 3).

2.3 Reference frame-specific differences in ERC

Significant ERC differences between allocentric and egocentric navigators in distinct frequency bands and time periods of the navigation task are illustrated in Figure 4 and Figure 5 for the anterior and the posterior network, respectively.

********** insert Figure 4 here **********

As shown in Figure 4, sustained ERC differences in the alpha band were found from the left motor to the left prefrontal cortex (LM->LPF) and the left prefrontal cortex to the left motor cortex (LPF->LM). Sustained ERC differences were also observed in the delta band from left prefrontal cortex to right prefrontal cortex (LPF->RPF) and around 25 Hz from the left and the right prefrontal cortex to the ACC (LPF->ACC & RPF->ACC).

Task-related ERC differences were observed during stimulus turns, with egocentric navigators demonstrating significantly increased ERC as compared to allocentric navigators between ACC and the left motor cortex (ACC<->LM), from

ACC to the right prefrontal cortex (ACC->RPF) in theta band and between right prefrontal cortex and right motor cortex (RPF<->RM) in the alpha band. Egocentric groups also showed significantly increased ERC in alpha band from the left motor cortex to the right motor cortex (LM->RM) in the straight segment before stimulus turn (bootstrapping, FDR-adjusted $p < 0.05$).

ERC differences in the delta and alpha band were found in the posterior network as showed in Figure 5 (bootstrapping, FDR-adjusted $p < 0.05$). Sustained significant ERC difference in alpha band between strategy groups were found between the left parietal cortex and left motor cortex (LP<->LM) and the left and right parietal cortex (LP<->RP) (bootstrapping, FDR-adjusted $p < 0.05$). Allocentric participants further demonstrated significantly stronger ERC in delta band from the left motor cortex to left parietal cortex (LM->LP) over all navigation segments (bootstrapping, FDR-adjusted $p < 0.05$). The RSC and the occipital cortex, crucial regions for spatial navigation, revealed significant strategy dependent ERCs with other brain areas (bootstrapping, FDR-adjusted $p < 0.05$). Allocentric navigators showed stronger ERC in the alpha band between the RSC and the right parietal cortex as well as the occipital cortex, and the right parietal cortex (RSC<->RP & Occ<->RP) especially during stimulus turns. ERC differences between the RSC and occipital cortex (RSC<->Occ) were revealed in the delta band for straight segments before and after the turn and in the alpha band during stimulus turns. Moreover, ERC between the RSC and the right motor cortex (RSC<->RM) was significantly stronger for egocentric participants (bootstrapping, FDR-adjusted $p < 0.05$).

********** insert Figure 5 here **********

3. Discussion

In this study, we found ERC flow in the delta (1–3.5 Hz), theta (4–7 Hz), alpha (8–13 Hz), and beta (14–30 Hz) frequency bands in the human navigation network during virtual path integration. The dominant frequency characteristics of this network were in line with previous EEG studies demonstrating theta power increases in the frontal cortex to co-vary with alpha power changes in the motor, parietal, and occipital cortices as well as the RSC [Lin et al., 2015; Chiu et al., 2012; Plank et al., 2010; Gramann et al., 2010]. Other studies using coherence analysis also revealed increased coherence of the theta and alpha frequency bands during navigation tasks [Li et al., 2009]. Using sdDTF we found direct Granger causal relationships between different brain regions that demonstrated task-related modulations and significant differences dependent on the reference frame that was used for spatial updating.

The results allow for a broad classification of two functionally distinct, but overlapping cortical networks. One network, the *anterior navigation network*, demonstrated significant ERC flows between anterior areas including the ACC and bilateral prefrontal cortices, extending to the motor and parietal cortices (see Figure 4). A second network, the *posterior navigation network*, included the motor cortex as well as the parietal and occipital cortices, and the RSC (see Figure 5). These results are in line with anatomical findings [Brodmann, 2006; Fuster, 2003;

Maguire, 2001; Morris et al., 2000; Vann et al., 2009] and underscore the central role of these regions within the navigation network.

3.1 Anterior navigation network

The frontal cortex is crucial for working memory functions and plays a central role in various tasks including, but not limited to, spatial orientation [Courtney et al., 1998; Curtis, 2006; Zanto et al., 2011]. Imaging studies have revealed that the demand of visuospatial working memory is reflected by increased activity within the prefrontal and the dorsolateral prefrontal cortices [Barbey et al., 2013]. In this study, we have shown theta connectivity between clusters of ICs with the cluster centroids located in or near the ACC and the right and left dorsolateral prefrontal cortices for both strategy groups (see Figure. 4). The positive correlation between the increased frontal theta power and the demanding navigation has been reported in the previous studies [Caplan et al., 2003; Kahana et al., 1999] and are in line with recent results indicating increased prefrontal cortex activity with more complex navigation decisions [Javadi et al., 2017]. Thus, the observed theta connectivity between the ACC and the right and left dorsolateral prefrontal cortices points to varying working memory demands during the spatial navigation task.

The dorsolateral prefrontal region further demonstrated connectivity with the motor cortex for both strategy groups. This finding is in line with the assumption that the dorsolateral prefrontal cortex is involved in various tasks requiring higher order motor planning and control [Cieslik et al., 2013; Rowe et al.,

2005]. Other studies have shown that first-person perspective navigation also activates the premotor cortex and parietal cortex, besides the dorsolateral prefrontal cortex [Baumgartner et al., 2008; Jäncke et al., 2009]. Our results support the assumption that information exchange between the dorsolateral frontal and ipsilateral motor cortices is independent of the reference frame used and that it may reflect the direction of attention to the visual motion stimuli [Curtis and D'Esposito, 2003].

Different aspects of the path integration task required working memory resources to maintain and update orientation changes with respect to the starting position. The neural basis for this aspect of spatial updating was provided through a network involving information flow between the ACC and dorsolateral prefrontal cortex in the theta and beta frequency bands. Imagined movement and integration of task-related movement information involved alpha connectivity between the prefrontal, motor, and parietal cortices.

3.2 Posterior navigation (RSC-related) network

In addition to the anterior navigation network, a posterior navigation network revealed the RSC to be causally connected with the motor cortex and the parietal and occipital cortices (see Figure 5). In our previous study, we found co-varying power changes in the alpha frequency band in the parietal and occipital cortices and the RSC, reflecting the involvement of these regions in spatial information processing [Lin et al., 2015]. The present study demonstrated this alpha rhythm to provide a causal connection between these areas. This posterior

navigation network, with the RSC as a hub connecting functionally different regions, plays a vital role in allocentric and egocentric spatial information processing.

The RSC has been implied as central to the navigation network [Byrne et al., 2007; Ino et al., 2007; Maguire, 2001; Rosenbaum et al., 2004; Vann et al., 2009], particularly with respect to the transformation of egocentric and allocentric information. Several authors suggest the RSC to be responsible for transforming idiothetic spatial information, such as visual flow and other self-motion cues, into an allocentric representation [Byrne et al., 2007; Dhindsa et al., 2014; Vann et al., 2009; Zhang et al., 2012]. In this study, we observed that the RSC was causally connected with the parietal and occipital cortices during path integration, mainly through modulations in the alpha frequency range. In addition, we observed that alpha connectivity between the RSC and the occipital cortex was sustained throughout the navigation period and more pronounced for allocentric navigators. Successful navigation required the participants to continuously maintain their position changes with respect to the origin of the passage. Sustained ERC flows between the RSC and occipital cortex during straight segments arguably reflect the engagement of continuous integration of visual information from a first-person perspective into an allocentric representation.

In contrast to straight segments that provided information on translational changes without changes in heading, stimulus turns provided information only on heading changes but not on changes in position. During rotations on the spot, the RSC revealed the strongest causal connectivity with the parietal cortex for

allocentric participants (see Figure 5). Baumann and Mattingley [2010] found that the medial parietal cortex was engaged in the computation of allocentric directions. Recently, Marchette et al. [2014] demonstrated BOLD activations in the RSC during encoding of allocentric heading directions. Taking these findings together, ERC flow in the alpha band between the RSC and parietal cortex is proposed to reflect the integration of changes in heading with respect to an allocentric heading direction. These findings support the idea that the RSC is crucial for allocentric information processing and that the connectivity between the RSC, occipital, and parietal cortices reflects network activity subserving the transformation of egocentric information into an allocentric representation based on heading information provided by the RSC itself.

In rats, the RSC was found to transmit spatial information to anterior brain regions, including the motor cortex, through direct anatomical connections [Shibata et al., 2004; White et al., 2011]. The human RSC is located within and adjacent to the dorsal posterior cingulate cortex, which shows extensive efferent and afferent connections with cortical areas that process visuospatial information and information on the orientation of the body in space via interaction with numerous premotor areas, including the cingulate motor area [Vogt et al., 2006]. Besides strategy-related connectivity patterns, delta flows between the RSC and the occipital cortex were found during the complete navigation phase for both strategy groups. The delta RSC–occipital cortex causal flow possibly reflects the processing of first-person perspective movement information that is fed from the occipital cortex into the RSC [Jacobs et al., 2010]. Thus, the present study further

supports the emerging idea that the RSC is not only specialized for transforming egocentric and allocentric information into different reference frames but also serves a more general function in spatial behavior requiring further investigation.

4. Limitation and Conclusion

Our work discovered a large-scale navigation network subserving spatial orientation on the basis of egocentric and allocentric SRFs. A number of caveats need to be noted regarding the current research. The first limitation is the data analysis. Since the signal-to-noise ratio is poor in EEG data, the relative processing methods are needed to extract the useful information from EEG. The analysing methods including pre-processing, noise removal, source separation and location were also required to estimate the functional causalities by SIFT. The second limitation is the subject size. This navigation network shown in this manuscript was gained through two sets of participants who finalized the designed tasks in the well-control laboratory.

The network can be differentiated into two functionally distinct but overlapping cortical networks: 1) an anterior navigation network, including the ACC and bilateral prefrontal cortices, extending to the motor and parietal cortices and 2) a posterior navigation network, with the RSC as the central hub connected with the motor, parietal, and occipital cortices. Spatial orienting recruited both the anterior network for spatial information retention and motion imagery/execution and the posterior network for processing and integration of visuospatial information. The RSC demonstrated strong alpha connectivity with the occipital

and parietal cortices most pronounced for allocentric participants, supporting the assumption that first-person sensory information is transformed into an allocentric spatial representation and vice versa through the RSC. This result strongly supports the assumption that egocentric and allocentric reference frames are active in parallel, rather than the assumption that only one reference frame is used to solve the task. The preferred use of one or the other SRF only modulates the strength of activation and connectivity with other brain areas.

5. Materials and Methods

5.1 Homing Task

We used a VR path integration task with passive transportation during environments with clear geometric structure and rich visual flow information (for a detailed description of the task please see Lin et al., 2015). Participants always started from the same position (marked by star in Figure 6A) in the VR scenario and were passively guided along different trajectories (as shown in Figure 6). All trajectories were composed of varying numbers of straight segments of the same length before and after a stimulus turn. All stimulus turns were 90° rotations on the spot, to the left or the right. The participants were asked to maintain their orientation during the navigation phase and to point back to the start position (marked by star in Figure 6A) at the end of a passage. The National Chiao Tung University (NCTU) ethics committee approved this study.

********** insert Figure 6 here **********

393

394 Each experimental block started with a baseline trial in which participants
395 experienced a random walk through the maze environment. First, for 2 s, they saw
396 a picture of an arrow pointing in any direction between −180° and 180°. Then,
397 they moved through the maze in a random manner, experiencing translations and
398 rotations for 1 min. The participants required to focus on the visual flow without
399 actively orienting. After the random walk period, a response arrow was displayed
400 one the screen and the participants were asked to adjust the angle of arrow to
401 match the pointing direction of the initially presented arrow. The participants
402 perceived comparable visual flow during experimental and baseline trials without
403 the need for active spatial updating during the baseline condition [Wolbers et al.,
404 2007].

405

406 **5.2 EEG Recording and Analysis**

407 Twenty-one right-handed male participants performed the task. Participants
408 were categorized as allocentric or egocentric navigators based on their responses
409 after each trial resulting in 9 allocentric and 12 egocentric navigators (mean
410 strategy-consistent adjustments = 98.4%, sd = 2.1%). EEG signals were recorded
411 using 64 electrodes placed in an elastic cap according to the extended 10-20
412 system. EEG data were acquired by the Scan NuAmps Express system
413 (Compumedics Ltd., VIC, Australia) referenced to Cz and digitized at 1 KHz and 32-
414 bit precision. All channels had impedances below 5 kΩ.

The recorded signals were analyzed with EEGLAB [Delorme and Makeig, 2004], first down-sampled to 250 Hz and then filtered to remove frequencies below 0.5 Hz and above 50 Hz. The acquired signals were re-referenced by the averaging values from the all channels. The filtered data were visually inspected and manually cleaned in the time and the channel domain. Short time periods with bursts of higher frequencies resembling muscle artifacts were manually marked and subsequently removed from the continuous data. Eye movements were not removed to allow independent component analysis (ICA) to decompose eye movement related activity. The channel data without any activity over longer time periods and the channel data with strong deviation from neighboring channels were indicated as “dead channels” and “noisy channels”, respectively. This criterion led to the removal of 4.4 channels (3.2 sd) per participant.

After removing artifacts, adaptive mixture independent component analysis (AMICA) [Palmer et al., 2008] was applied to decompose EEG data into statistically maximally independent time source series (independent components, ICs), allowing further estimation of information flow between ICs. To approximate the spatial origin of IC activations, an equivalent current dipole model was computed for each IC in a four-shell spherical head model using DIPFIT2 routines [Oostenveld and Oostendorp, 2002]. Subsequently, individual ICs were clustered across participants based on the time course of event-related potentials (ERPs), mean IC log spectra, equivalent dipole locations, event-related spectral perturbation (ERSP), and intertrial coherence (ITC), replicating the setting of K-

means clustering used in previous studies [Gramann et al., 2010; Chiu et al., 2012; Lin et al., 2015].

From an initial set of 1,209 ICs of all participants, 897 ICs with a residual variance of the equivalent dipole model of less than 15% were clustered. Finally, nine clusters with a total of 171 ICs were identified as brain sources based on their locations in or near the grey matter of the head model. The reconstruction of sources based on EEG data provides only an approximation of the unknown source locations and any description of cortical structures is based on an estimate of the real source location. The centroids of these clusters were located throughout the brain including brain regions as shown in Table I.

********** insert Table I here **********

5.3 Causality Analysis

IC time series were analyzed using the Source Information Flow Toolbox (SIFT) [Delorme et al., 2011; Mullen et al., 2010], an open source toolbox for brain connectivity analysis. Based on the concept of causal influence as put forward by Granger [1969], direct directed transfer function (dDTF) [Korzeniewska et al., 2003], a measurement based on vector autoregressive (VAR) models was used to estimate the directionality as well as the intensity of causal interactions in brain dynamics [Babiloni et al., 2005; Deshpande et al., 2009; Ginter et al., 2005; Kus and Blinowska, 2008]. This approach determines the frequency band in which the causal influence occurs and the short-time version of the algorithm [sdDTF;

460 Korzeniewska et al., 2008], and related methods [Ding et al., 2000] are capable of
461 capturing the temporal evolution of direct causal influences between brain regions
462 and have been successfully applied to evaluate causal influences in
463 electrophysiological signals such as EEG [Iversen et al., 2014; Markman et al., 2013]
464 and ECoG [Korzeniewska et al., 2003; Mullen et al., 2011].

465 The IC signals were first down-sampled to 128 Hz and then normalized in a
466 2-step procedure. In the first step, data were normalized across time for each
467 epoch by subtracting the mean and dividing by the standard deviation of the epoch
468 data. The second step was the ensemble normalization of data across epochs; here,
469 the ensemble average was subtracted from the data and then the result was
470 divided by the ensemble standard deviation. Subsequently, a parametric linear
471 vector autoregressive (VAR) model was fitted to the IC signals on the basis of a
472 multivariate least-squares approach. The VAR model assumes that the value of the
473 multi-channel time series at a given time point depends on the values of a certain
474 number of previous time points. The number of previous points was optimally
475 selected as the model order using the Akaike Information Criterion [Akaike, 1974].
476 The "ARfit" routine in SIFT was applied to the IC data to estimate the VAR model of
477 order 15 with a sliding window of 500 ms and a step size of 50 ms. Subsequently,
478 the model was validated by tests of residual whiteness and stability [Lütkepohl,
479 2005]. Based on the model coefficients, the short-time dDTF was estimated to
480 measure the causal information transferred between ICs in the frequency band of
481 1–50 Hz for each overlapping sliding window, reflecting the dynamic time–
482 frequency information flow between the brain sources.

5.4 Statistical Analysis

The two-way ANOVA statistical test and post hoc Wilcoxon signed-rank test were introduced to test the behavioural information ('strategy' x 'end Position'). A mix-model ANOVA statistic showed that the turning direction had no impact on homing angles, thus left and right turning trials were merged to investigate homing performance (homing angles) for both strategy groups.

Following the estimation of causality, phase randomization, a non-parametric surrogate statistical test was applied with FDR correction on each time-frequency point of the sdDTF matrix to find significant ($p<0.05$) non-zero causality between signals. The phase randomization method generated a null surrogate distribution containing zero-information-flow by randomizing the phases of IC signals but preserving their amplitudes and then tested the measured causality against this surrogate distribution for each time-frequency point [Theiler et al., 1992]. To further measure significant causal flow as compared to the baseline condition, bootstrapping tests with FDR correction were applied to each time-frequency point of sdDTF matrix. To this end the causality values of the baseline condition were subtracted from causality values of navigation segments and the difference was averaged across subjects resulting in an event-related causality (ERC) matrix. Non-significant ERC-values were masked (using green color) and only significantly deviations from the baseline condition after FDR correction ($p<0.05$) were color-coded (with blue colors for negative values and red colors for positive values). For the analysis of differences between strategy groups (egocentric vs. allocentric navigators), bootstrapping test and FDR correction were applied to

each time-frequency point of ERC of allocentric and egocentric navigators and significant ERC-differences were color-coded as described for the individual ERCs.

Acknowledgments

This work was supported in part by the UST-UCSD International Center of Excellence in Advanced Bio-engineering sponsored by the Taiwan National Science Council I-RiCE Program under Grant Number: MOST 103-2911-I-009-101, in part by MOST 103-2627-E-009-001, in part by MOST 105-2221-E-009-069, in part by the Aiming for the Top University Plan, under Contract: 106W963, and in part by the Army Research Laboratory: W911NF-10-2-0022.

Reference

Akaike H (1974): A new look at the statistical model identification. IEEE Trans Automat Contr 19:716–723.

Babiloni F, Cincotti F, Babiloni C, Carducci F, Mattia D, Astolfi L, Basilisco A, Rossini PM, Ding L, Ni Y, Cheng J, Christine K, Sweeney J, He B (2005): Estimation of the cortical functional connectivity with the multimodal integration of high-resolution EEG and fMRI data by directed transfer function. Neuroimage 24:118–131.

Barbey AK, Koenigs M, Grafman J (2013): Dorsolateral prefrontal contributions to human working memory. Cortex 49:1195–1205.

Baumann O, Mattingley JB (2010): Medial parietal cortex encodes perceived heading direction in humans. J Neurosci 30:12897–12901.

Baumgartner T, Speck D, Wettstein D, Masnari O, Beeli G, Jäncke L (2008): Feeling present in arousing virtual reality worlds: prefrontal brain regions differentially orchestrate presence experience in adults and children. Front Hum Neurosci 2:8.

Brodmann K (2006): Brodmann's Localisation in the Cerebral Cortex The Principles of Comparative Localisation in the Cerebral Cortex Based on Cytoarchitectonics 3rd ed. New York: Springer.

Byrne P, Becker S, Burgess N (2007): Remembering the past and imagining the future: a neural model of spatial memory and imagery. Psychol Rev 114:340–375.

Caplan JB, Madsen JR, Schulze-Bonhage A, Aschenbrenner-Scheibe R, Newman EL, Kahana MJ (2003): Human theta oscillations related to sensorimotor integration and spatial learning. J Neurosci 23:4726–4736.

Chiu T-C, Gramann K, Ko L-W, Duann J-R, Jung T-P, Lin C-T (2012): Alpha modulation in parietal and retrosplenial cortex correlates with navigation performance. Psychophysiology 49:43–55.

Cieslik EC, Zilles K, Caspers S, Roski C, Kellermann TS, Jakobs O, Langner R, Laird AR, Fox PT, Eickhoff SB (2013): Is there “one” DLPFC in cognitive action control? Evidence for heterogeneity from co-activation-based parcellation. Cereb Cortex 23:2677–2689.

Cohen YE, Andersen RA (2002): A common reference frame for movement plans in the posterior parietal cortex. Nat Rev Neurosci 3:553–562.

Committeri G, Galati G, Paradis A-L, Pizzamiglio L, Berthoz A, LeBihan D (2004): Reference frames for spatial cognition: different brain areas are involved in viewer-, object-, and landmark-centered judgments about object location. J Cogn Neurosci 16:1517–35.

Courtney SM, Petit L, Maisog JM, Ungerleider LG, Haxby J V (1998): An area specialized for spatial working memory in human frontal cortex. Science 279:1347–1351.

Curtis CE (2006): Prefrontal and parietal contributions to spatial working memory. Neuroscience 139:173–180.

Curtis CE, D’Esposito M (2003): Persistent activity in the prefrontal cortex during working memory. Trends in Cognitive Sciences 7:415-423.

Delorme A, Makeig S (2004): EEGLAB: An open source toolbox for analysis of single-trial EEG dynamics including independent component analysis. J Neurosci Methods 134:9–21.

Delorme A, Mullen T, Kothe C, Akalin Acar Z, Bigdely-Shamlo N, Vankov A, Makeig S (2011): EEGLAB, SIFT, NFT, BCILAB, and ERICA: New tools for advanced EEG processing. Comput Intell Neurosci 2011:10.

Deshpande G, LaConte S, James GA, Peltier S, Hu X (2009): Multivariate granger causality analysis of fMRI data. Hum Brain Mapp 30:1361–1373.

Dhindsa K, Drobinin V, King J, Hall GB, Burgess N, Becker S (2014): Examining the role of the temporo-parietal network in memory, imagery, and viewpoint transformations. Front Hum Neurosci 8:709.

Ding M, Bressler SL, Yang W, Liang H (2000): Short-window spectral analysis of cortical event-related potentials by adaptive multivariate autoregressive modeling: data preprocessing, model validation, and variability assessment. Biol Cybern 83:35–45.

Doeller CF, Barry C, Burgess N (2010): Evidence for grid cells in a human memory network. Nature 463:657–661.

Ekstrom AD, Kahana MJ, Caplan JB, Fields TA, Isham EA, Newman EL, Fried I (2003): Cellular networks underlying human spatial navigation. Nature 425:184–188.

Ekstrom, AD, Aiden EGFA, Iaria G (2014): A critical review of the allocentric spatial representation and its neural underpinnings: toward a network-based perspective. Frontiers in human neuroscience 8.

Fuster JM (2003): Frontal lobe and cognitive development. J Neurocytol 31:373–85.

Ginter J, Blinowska KJ, Kamiński M, Durka PJ, Pfurtscheller G, Neuper C (2005): Propagation of EEG activity in the beta and gamma band during movement imagery in humans. Methods Inf Med 44:106–113.

Goeke CM, König P, Gramann K (2013): Different strategies for spatial updating in yaw and pitch path integration. Front Behav Neurosci 7:5.

Goeke, CM, Kornpetpanee, S, Köster, M, Fernández-Revelles, AB, Gramann, K, & König, P (2015). Cultural background shapes spatial reference frame proclivity. *Scientific reports*, *5*.

Gomez A, Cerles M, Rousset S, Rémy C, Baciu M (2014): Differential hippocampal and retrosplenial involvement in egocentric-updating, rotation, and allocentric processing during online spatial encoding: an fMRI study. Front Hum Neurosci 8:150.

599 Gramann K, Müller HJ, Schönebeck B, Debus G (2006): The neural basis of ego-
600 and allocentric reference frames in spatial navigation: evidence from spatio-
601 temporal coupled current density reconstruction. Brain Res 1118:116–129.

602 Gramann K, Müller HJ, Eick E-M, Schönebeck B (2005): Evidence of separable
603 spatial representations in a virtual navigation task. J Exp Psychol Hum
604 Percept Perform 31:1199–1223.

605 Gramann K, Onton J, Riccobon D, Mueller HJ, Bardins S, Makeig S (2010): Human
606 brain dynamics accompanying use of egocentric and allocentric reference
607 frames during navigation. J Cogn Neurosci 22:2836–2849.

608 Gramann K, El Sharkawy J, Deubel H (2009): Eye-movements during navigation
609 in a virtual tunnel. Int J Neurosci 119:1755–1778.

610 Gramann, K., Wing, S., Jung, T. P., Viirre, E., & Riecke, B. E. (2012). Switching
611 spatial reference frames for yaw and pitch navigation. Spatial Cognition &
612 Computation, 12(2-3), 159-194.

613 Granger CWJ (1969): Investigating Causal Relations By Econometric Models and
614 Cross-Specteral Methods. Econometrica 37:424–438.

615 Hartley T, Maguire E a, Spiers HJ, Burgess N (2003): The well-worn route and the
616 path less traveled: distinct neural bases of route following and wayfinding in
617 humans. Neuron 37:877–888.

618 Howard LR, Javadi AH, Yu Y, Mill RD, Morrison LC, Knight R, Loftus MM, Staskute
619 L, Spiers HJ (2014): The hippocampus and entorhinal cortex encode the
620 path and euclidean distances to goals during navigation. Curr Biol 24:1331–
621 1340.

622 Ino T, Doi T, Hirose S, Kimura T, Ito J, Fukuyama H (2007): Directional
623 disorientation following left retrosplenial hemorrhage: A case report with
624 fMRI studies. Cortex 43:248–254.

625 Iversen JR, Ojeda A, Mullen T, Plank M, Snider J, Cauwenberghs G, Poizner H
626 (2014): Causal analysis of cortical networks involved in reaching to spatial

627 targets. In: . 2014 36th Annual International Conference of the IEEE
628 Engineering in Medicine and Biology Society. IEEE. pp 4399–4402.

629 Jacobs J, Korolev IO, Caplan JB, Ekstrom AD, Litt B, Baltuch G, Fried I, Schulze-
630 Bonhage A, Madsen JR, Kahana MJ (2010): Right-lateralized brain
631 oscillations in human spatial navigation. J Cogn Neurosci 22:824–836.

632 Jacobs J, Weidemann CT, Miller JF, Solway A, Burke JF, Wei X-X, Suthana N,
633 Sperling MR, Sharan AD, Fried I, Kahana MJ (2013): Direct recordings of
634 grid-like neuronal activity in human spatial navigation. Nat Neurosci
635 16:1188–1190.

636 Jäncke L, Cheetham M, Baumgartner T (2009): Virtual reality and the role of the
637 prefrontal cortex in adults and children. Frontiers in Neuroscience 3:9-52.

638 Javadi AH, Emo B, Howard L, Zisch F, Yu Y, Knight R, Joao PS and Spiers HJ
639 (2017). Hippocampal and prefrontal processing of network topology to
640 simulate the future. Nature Communications 14652.

641 Kahana MJ, Sekuler R, Caplan JB, Kirschen M, Madsen JR (1999): Human theta
642 oscillations exhibit task dependence during virtual maze navigation. Nature
643 399:781–784.

644 Klatzky R (1998): Allocentric and egocentric spatial representa- tions:
645 Definitions, distinctions, and interconnections. In: Freksa C, Habel C,
646 Wender KF, editors. Spatial cognition: An Interdis- ciplinary Approach to
647 Representation and Processing of Spatial Knowledge. Berlin: Springer-
648 Verlag. pp 1–17.

649 Korzeniewska A, Crainiceanu CM, Kuś R, Franaszczuk PJ, Crone NE (2008):
650 Dynamics of event-related causality in brain electrical activity. Hum Brain
651 Mapp 29:1170–1192.

652 Korzeniewska A, Mańczak M, Kamiński M, Blinowska KJ, Kasicki S (2003):
653 Determination of information flow direction among brain structures by a
654 modified directed transfer function (dDTF) method. J Neurosci Methods
655 125:195–207.

Kus R, Blinowska K (2008): Transmission of information during continuous attention test. Acta Neurobiol Exp 68:103–112.

Li Y, Umeno K, Hori E, Takakura H, Urakawa S, Ono T, Nishijo H (2009): Global synchronization in the theta band during mental imagery of navigation in humans. Neurosci Res 65:44–52.

Lin C-T, Chiu T-C, Gramann K (2015): EEG Correlates of Spatial Orientation in the Human Retrosplenial Complex. NeuroImage doi:10.1016/j.neuroimge.2015.07.007.

Lütkepohl H (2005): New Introduction to Multiple Time Series Analysis. Berlin/Heidelberg: Springer-Verlag.

Maguire EA (2001): The retrosplenial contribution to human navigation: a review of lesion and neuroimaging findings. Scand J Psychol 42:225–238.

Maguire EA, Burgess N, Donnett JG, Frackowiak RS, Frith CD, O'Keefe J (1998): Knowing where and getting there: a human navigation network. Science 280:921–924.

Marchette S a, Vass LK, Ryan J, Epstein R a (2014): Anchoring the neural compass: coding of local spatial reference frames in human medial parietal lobe. Nat Neurosci 17:1598-1606.

Markman T, Liu C, Chien J, Crone N, Zhang J, Lenz F (2013): EEG analysis reveals widespread directed functional interactions related to a painful cutaneous laser stimulus. J Neurophysiol 110:2440–2449.

Morris R, Paxinos G, Petrides M (2000): Architectonic analysis of the human retrosplenial cortex. J Comp Neurol 421:14–28.

Mullen T, Delorme A, Kothe C, Makeig S (2010): An electrophysiological information flow toolbox for EEGLAB. Biol Cybern 83:35-45.

Mullen T, Acar ZA, Worrell G, Makeig S (2011): Modeling cortical source dynamics and interactions during seizure. In: . Proceedings of the Annual

683 International Conference of the IEEE Engineering in Medicine and Biology
684 Society, EMBS pp 1411–1414.

685 Oostenveld R, Oostendorp TF (2002): Validating the boundary element method
686 for forward and inverse EEG computations in the presence of a hole in the
687 skull. Hum Brain Mapp 17:179–192.

688 Palmer JA, Makeig S., Delgado K. K., Rao B. D. (2008): Newton method for the ICA
689 mixture model, In: . Proceedings of the Annual IEEE International
690 Conference on Acoustics, Speech and Signal Processing (Las Vegas, NV:),
691 1805–1808.

692 Palva S, Palva JM (2011): Functional roles of alpha-band phase synchronization
693 in local and large-scale cortical networks. Frontiers in Psychology.

694 Plank M, Müller H, Onton J, Makeig S, Gramann K (2010): Human EEG correlates
695 of spatial navigation within egocentric and allocentric reference frames. In:
696 Hölscher C, Shipley TF, Olivetti Belardinelli M, Bateman JA, Newcombe NS,
697 editors. Spatial Cognition VII. Springer, Berlin:Springer-Verlag. pp. 191–206.

698 Ramos-Loyo J, Sanchez-Loyo LM (2011): Gender differences in EEG coherent
699 activity before and after training navigation skills in virtual environments.
700 Hum Physiol 37:700–707.

701 Rosenbaum RS, Ziegler M, Winocur G, Grady CL, Moscovitch M (2004): “I have
702 often walked down this street before”: fMRI studies on the hippocampus
703 and other structures during mental navigation of an old environment.
704 Hippocampus 14:826–835.

705 Rowe JB, Stephan KE, Friston K, Frackowiak RSJ, Passingham RE (2005): The
706 prefrontal cortex shows context-specific changes in effective connectivity to
707 motor or visual cortex during the selection of action or colour. Cereb Cortex
708 15:85–95.

709 Sauseng P, Klimesch W, Schabus M, Doppelmayr M (2005): Fronto-parietal EEG
710 coherence in theta and upper alpha reflect central executive functions of
711 working memory. Int J Psychophysiol 57:97–103.

712 Seubert J, Humphreys GW, Muller HJ, Gramann K (2008): Straight after the turn:
713 the role of the parietal lobes in egocentric space processing. Neurocase
714 14:204–219.

715 Shibata H, Kondo S, Naito J (2004): Organization of retrosplenial cortical
716 projections to the anterior cingulate, motor, and prefrontal cortices in the
717 rat. Neurosci Res 49:1–11.

718 Siegel M, Donner TH, Engel AK (2012): Spectral fingerprints of large-scale
719 neuronal interactions. Nat Rev Neurosci 13:121–134.

720 Theiler J, Eubank S, Longtin A, Galdrikian B, Doyne Farmer J (1992): Testing for
721 nonlinearity in time series: the method of surrogate data. Physica D:
722 Nonlinear Phenomena 58:77-94

723 Vann SD, Aggleton JP, Maguire EA (2009): What does the retrosplenial cortex do?
724 Nat Rev Neurosci 10:792–802.

725 Vogt BA, Vogt L, Laureys S (2006): Cytology and functionally correlated circuits
726 of human posterior cingulate areas. Neuroimage 29:452–466.

727 White BR, Bauer AQ, Snyder AZ, Schlaggar BL, Lee JM, Culver JP (2011): Imaging
728 of functional connectivity in the mouse brain. PLoS One 6.

729 Whitlock JR, Sutherland RJ, Witter MP, Moser M-B, Moser EI (2008): Navigating
730 from hippocampus to parietal cortex. Proc Natl Acad Sci U S A 105:14755–
731 14762.

732 Wolbers T, Büchel C (2005): Dissociable retrosplenial and hippocampal
733 contributions to successful formation of survey representations. J Neurosci
734 25:3333–3340.

735 Wolbers T, Wiener JM, Mallot HA, Büchel C (2007): Differential recruitment of
736 the hippocampus, medial prefrontal cortex, and the human motion complex
737 during path integration in humans. J Neurosci 27:9408–9416.

738 Zaehle T, Jordan K, Wüstenberg T, Baudewig J, Dechent P, Mast FW (2007): The
739 neural basis of the egocentric and allocentric spatial frame of reference.
740 Brain Res 1137:92–103.

741 Zanto TP, Rubens MT, Thangavel A, Gazzaley A (2011): Causal role of the
742 prefrontal cortex in top-down modulation of visual processing and working
743 memory. Nat Neurosci 14:656–661.

744 Zhang H, Copara M, Ekstrom AD (2012): Differential recruitment of brain
745 networks following route and cartographic map learning of spatial
746 environments. PLoS One 7:e44886.

747

748

749

750

751

752

753

754

755

756

757

758

759

760

761 **Figure Legend**

762 **Figure 1:** (A) Circular mean homing responses for Allocentric and Egocentric at
763 the end position of a-i and a-i. Dotted gray line: Allocentric, solid gray line:
764 Egocentric, dotted black line: mean homing response across Allocetric, solid black
765 line: mean homing response across Egocentric, black ticks: correct homing angles
766 for Allocentric and Egocentric. (B) Mean homing angles and errors in different end
767 position. Blue line: Egocentric, red line: Allocentric, black line: expected homing
768 response.

769

770 **Figure 2:** Time–frequency distribution of significant event-related causality (ERC)
771 flow from each cluster (columns) to other clusters (rows) for the anterior
772 navigation network. Because ERC flow was baseline-corrected, values range from
773 -1 to 1 instead of 0 (no granger causal flow) to 1 (maximum granger causal flow).
774 The scale for x and y axes is labeled in the bottom right of the figure. The bottom
775 row shows the sequential passage steps for both strategy groups: (straight)
776 passively moving forward by following the guiding arrow, (decelerate)
777 approaching the turning point and slowing down for turning, (turn) turning on the
778 spot, (straight) following the guiding arrow and moving forward again, and (end)
779 approaching the end and slowing down to stop. ACC, anterior cingulate cortex; LPF,
780 left prefrontal cortex; RPF, right prefrontal cortex; LM, left motor cortex; RM, right
781 motor cortex.

782

783 **Figure 3:** Time–frequency distribution of significant event-related causality (ERC)

784 flow from each cluster (columns) to other clusters (rows) for the posterior
785 navigaiton network. The bottom row shows the sequential passage steps for both
786 strategy groups: (straight) passively moving forward by following the guiding
787 arrow, (decelerate) approaching the turning point and slowing down for turning,
788 (turn) turning on the spot, (straight) following the guiding arrow and moving
789 forward again, and (end) approaching the end and slowing down to stop. LM, left
790 motor cortex; RM, right motor cortex; LP, left parietal cortex; RP, right parietal
791 cortex; RSC, retrosplenial complex; Occ, occipital cortex.
792
793 **Figure 4:** Time–frequency distribution of significant differences in event-related
794 causality (ERC) flow for the anterior navigation network computed by subtracting
795 ERC of egocentric participants from ERC of allocentric participants. The figure
796 layout is same as Figure 3. ACC, anterior cingulate cortex; LPF, left prefrontal cortex;
797 RPF, right prefrontal cortex; LM, left motor cortex; RM, right motor cortex.
798
799 **Figure 5:** Time–frequency distribution of significant differences in event-related
800 causality (ERC) flow for the posterior navigation network computed by
801 subtracting ERC of egocentric participants from ERC of allocentric participants.
802 The figure layout is same as Figure 3. LM, left motor cortex; RM, right motor cortex;
803 LP, left parietal cortex; RP, right parietal cortex; RSC, retrosplenial complex; Occ,
804 occipital cortex.
805
806 **Figure 6:** An illustration of the experimental design. (A) The virtual maze was a

grid-like navigation environment with irregular stonewalls and roads. The participants were guided along different possible paths (one example indicated by the gray dotted line) from the starting location (star) to an end position (circle). (B) Illustration of homing responses of the allocentric (dark gray head) and egocentric (light gray head) participants for a rightward turn. The homing directions for such a rightward path differed between the strategy groups, with the egocentric participants pointing back and to their right and the allocentric participants pointing back and to their left. (C) Screenshots of the homing task. The homing task required the participants to maintain their orientation during the navigation phase for 6–14 s depending on the path length until the end position was reached. After the navigation phase, a 3D homing arrow was displayed and the participants were required to point the homing direction by adjusting the arrow.

Supplementary Figure 1: Time–frequency distribution of significant ERC flow from each cluster (columns) to other clusters (rows) for all selected clusters. Figure layout is the same as Figure. 2. ACC, anterior cingulate cortex; LF, left prefrontal cortex; RF, right prefrontal cortex; LM, left motor cortex; RM, right motor cortex; LP, left parietal cortex; RP, right parietal cortex; RSC, retrosplenial complex; Occ, occipital cortex.

830

831 **Figures**

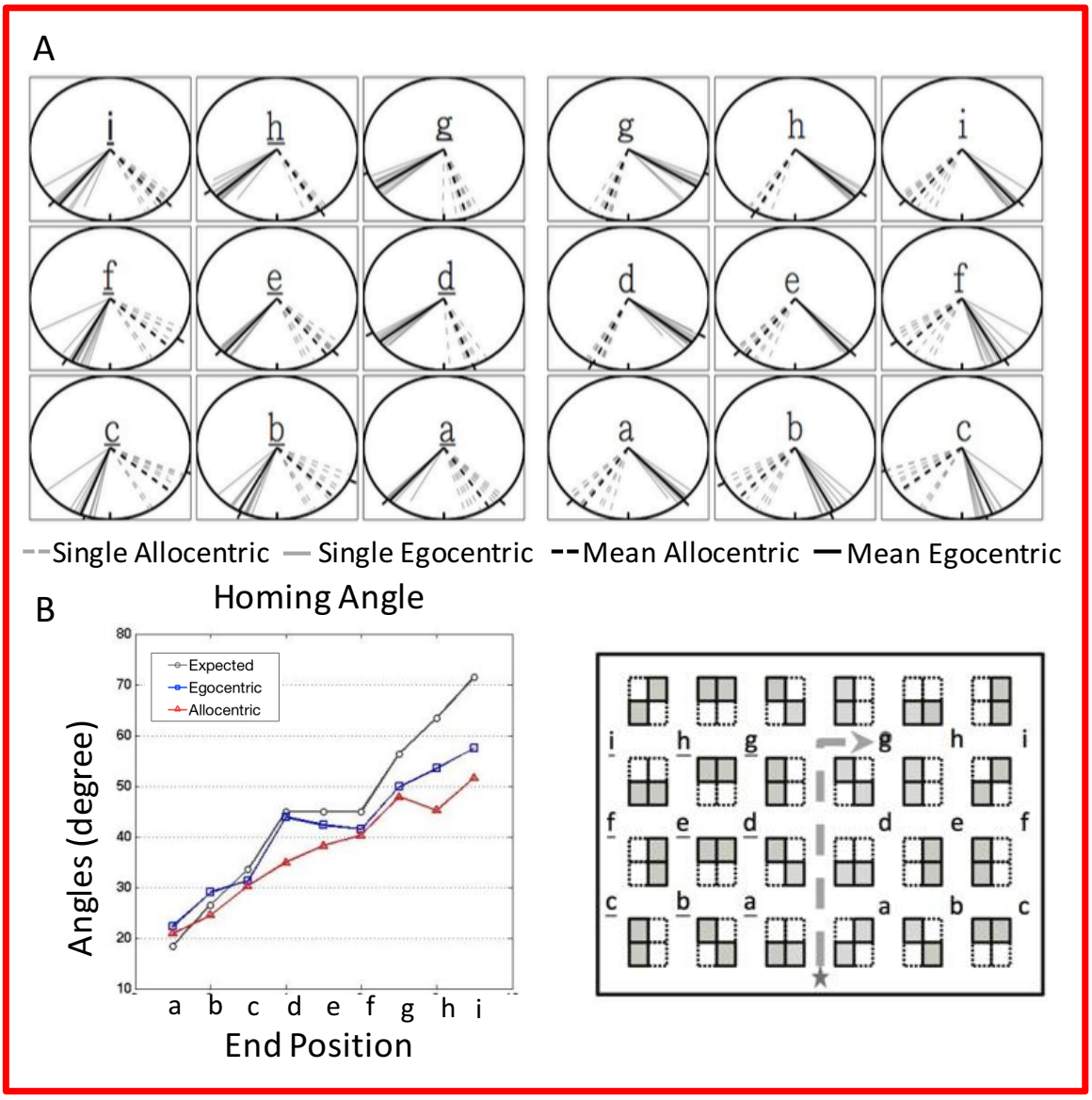

832

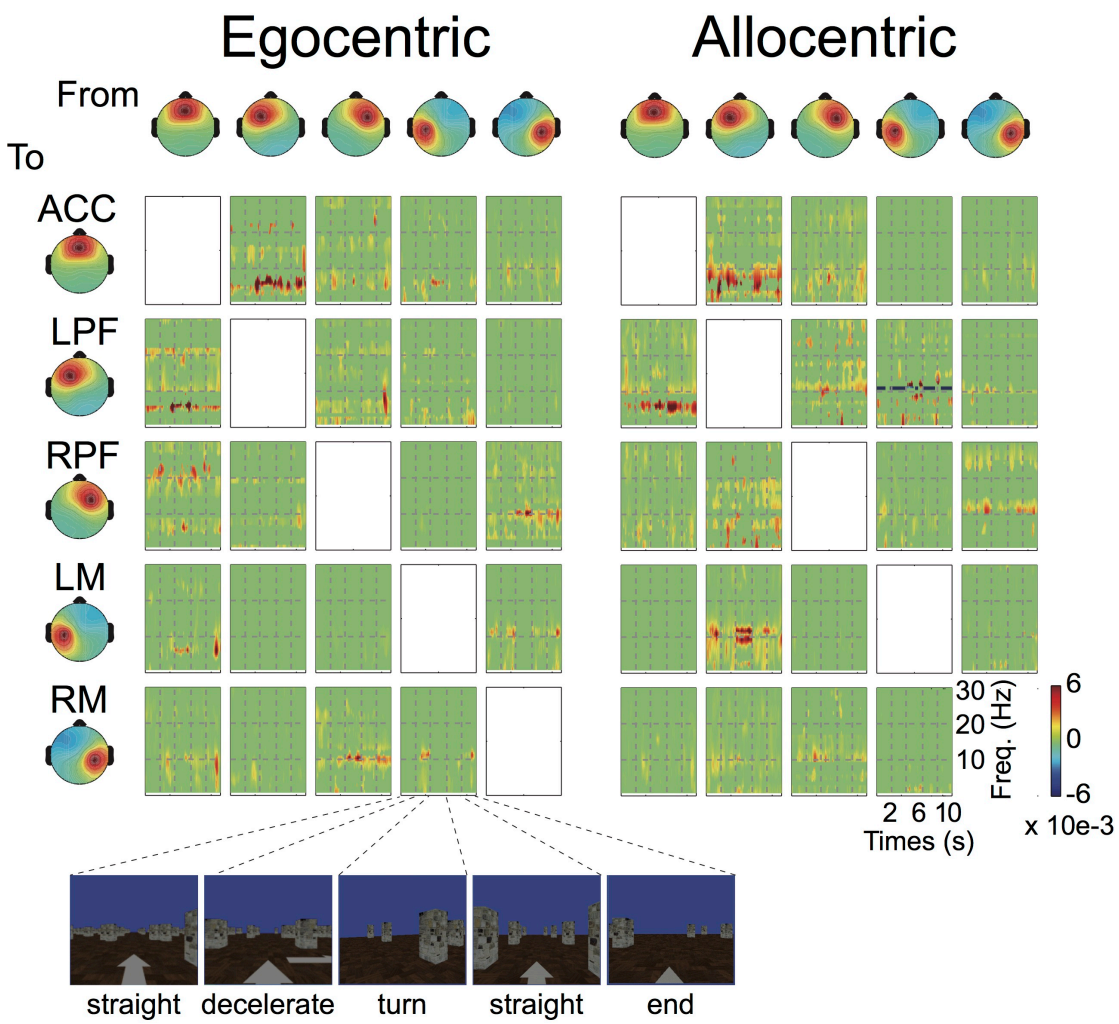
Egocentric
Allocentric
From
To
ACC
LPF
RPF
LM
RM
30
20
10
Freq. (Hz)
6
0
-6
x 10e-3
2 6 10
Times (s)
straight
decelerate
turn
straight
end

833

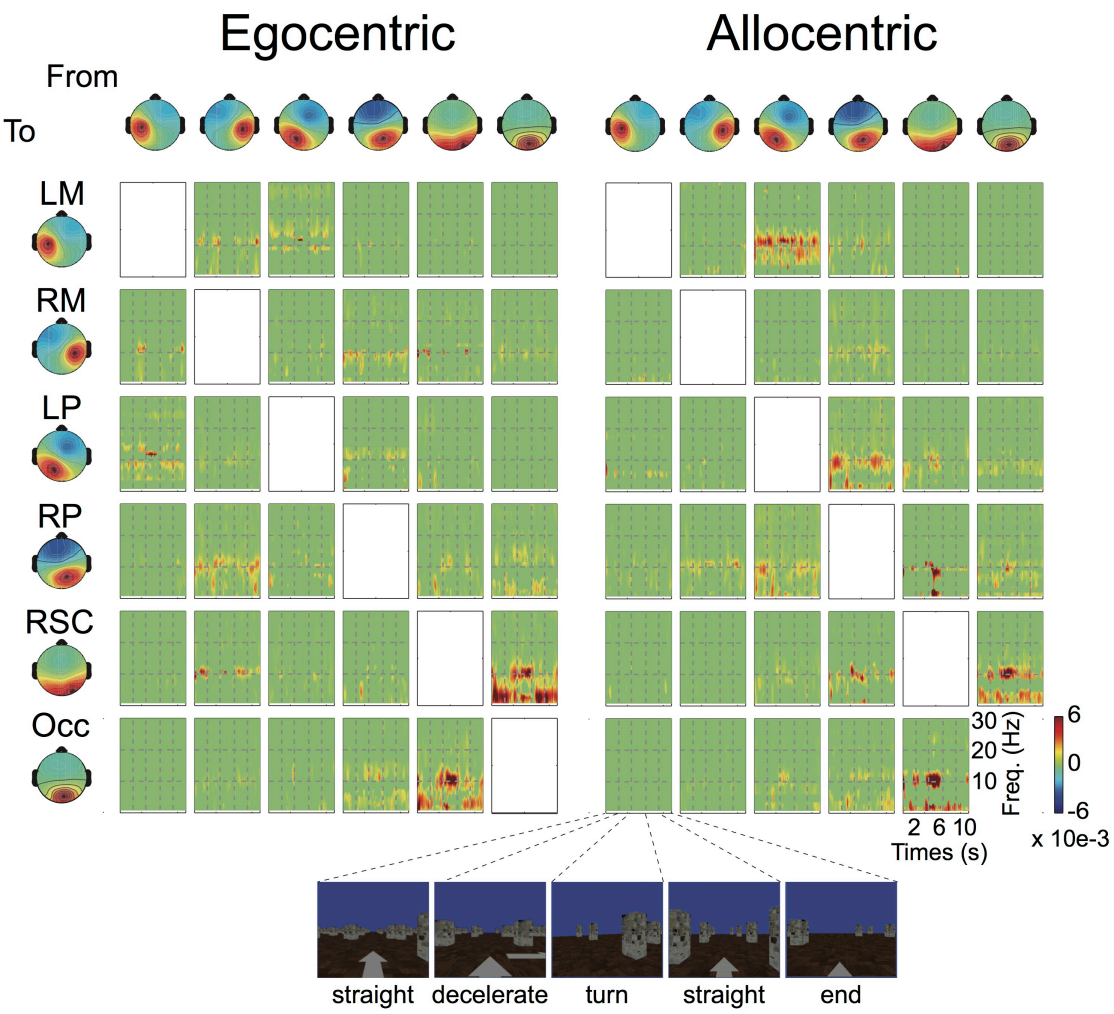
Egocentric
Allocentric
From
To
LM
RM
LP
RP
RSC
Occ
30
20
10
Freq. (Hz)
2 6 10
Times (s)
6
0
-6
x 10e-3
straight
decelerate
turn
straight
end

834

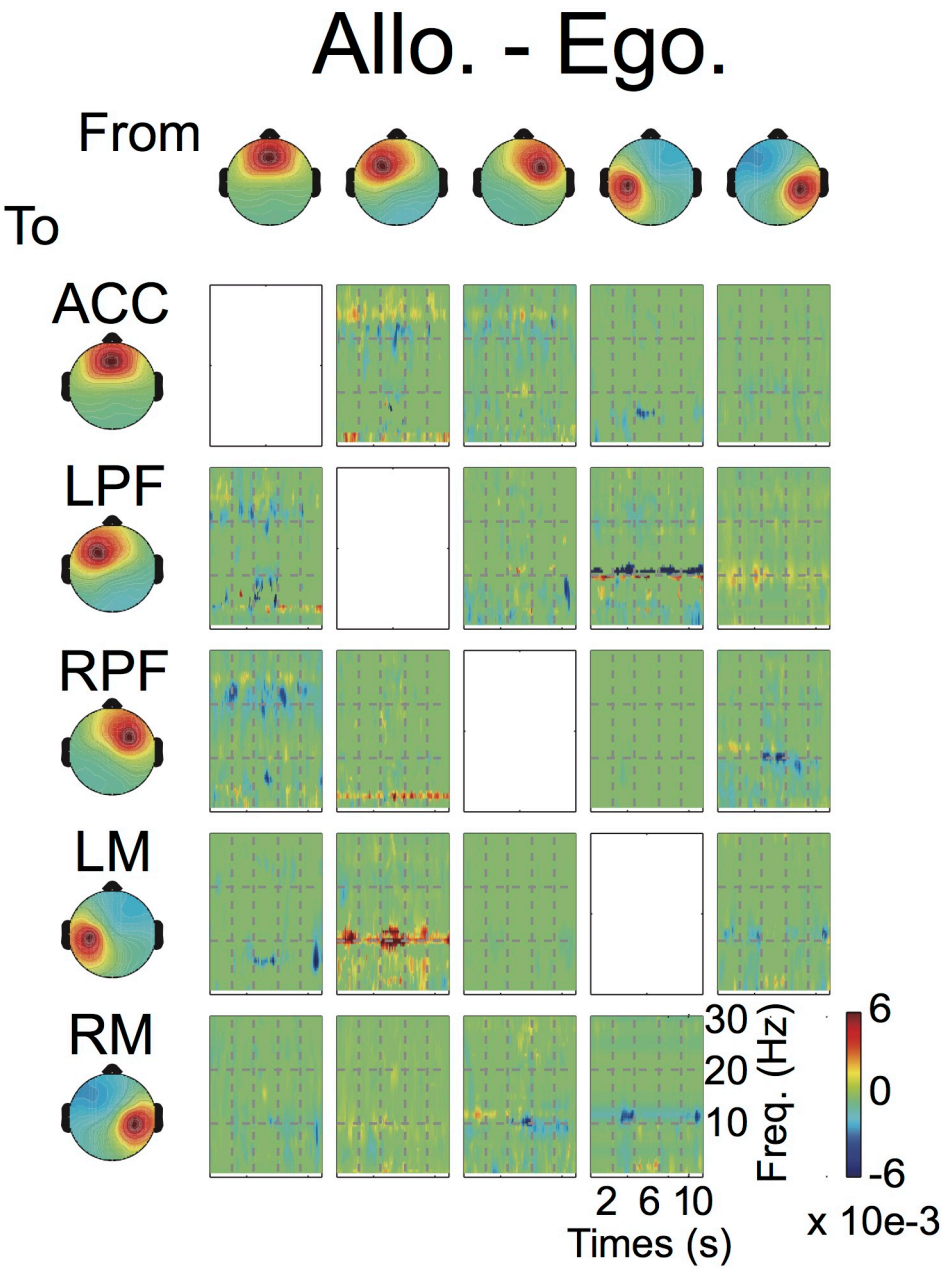
Allo. - Ego.
From
To
ACC
LPF
RPF
LM
RM
30
20
10
Freq. (Hz)
2 6 10
Times (s)
6
0
-6
x 10e-3

835

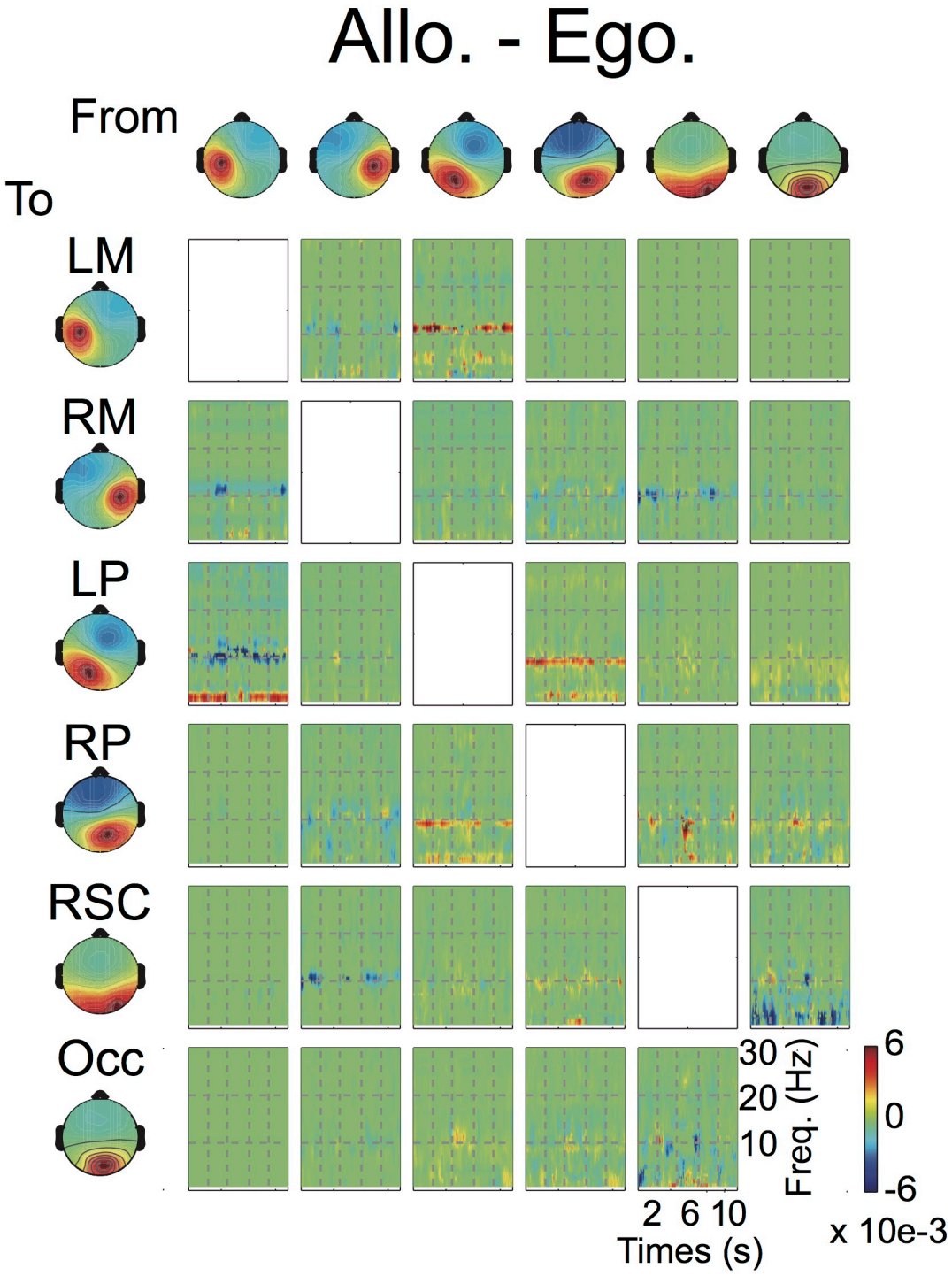
Allo. - Ego.
From
To
LM
RM
LP
RP
RSC
Occ
30
20
10
Freq. (Hz)
2 6 10
Times (s)
6
0
-6
x 10e-3

836

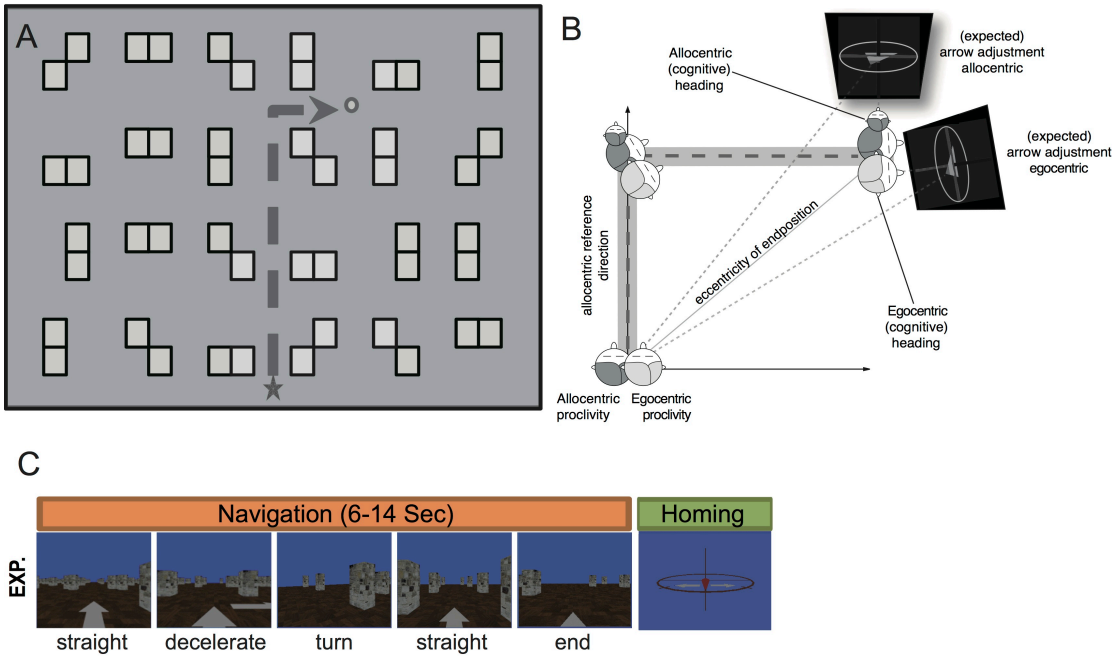

837

838

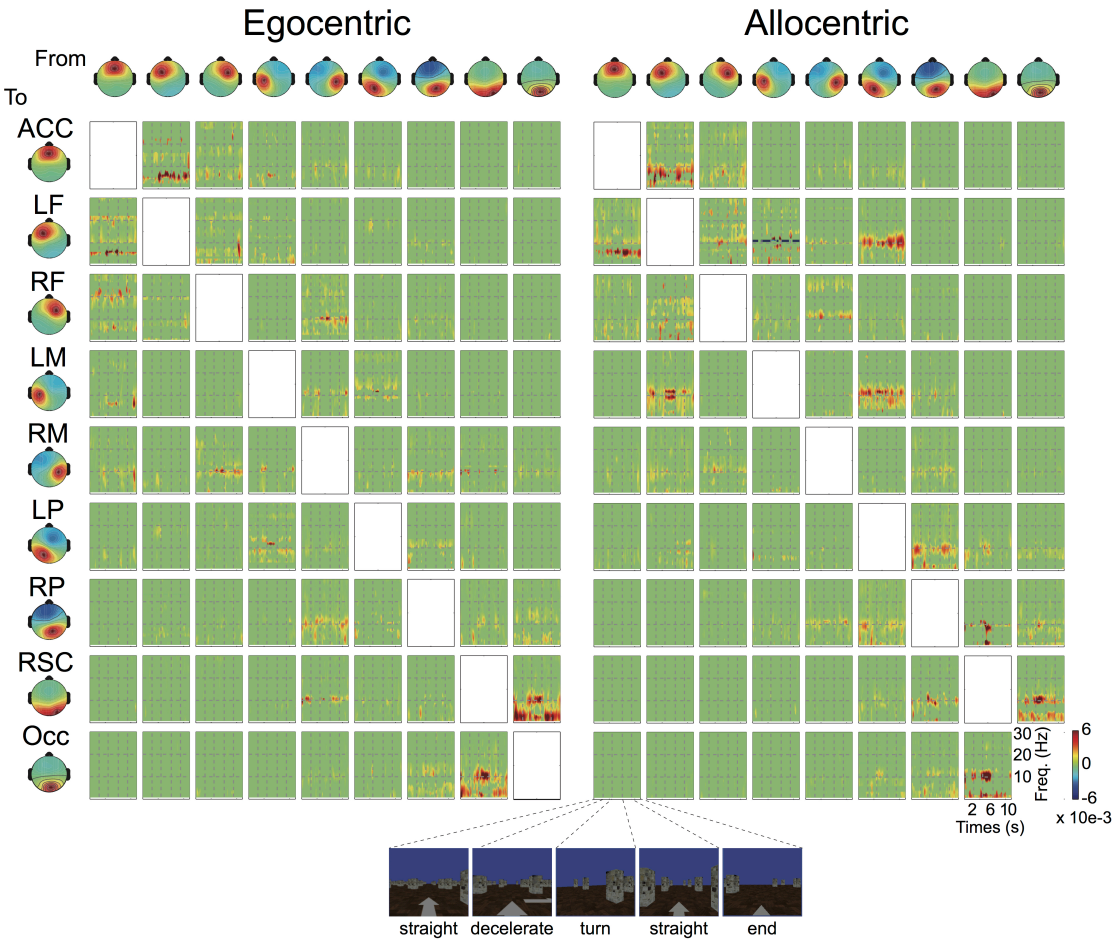

839

840

841 **Tables**

842 Table I Centroids of IC clusters and the brain region

	X	Y	Z	Brain Region
Cls 1	-1	37	33	anterior cingulate cortex (ACC)
Cls 2	-22	9	40	left prefrontal cortex (LPF)
Cls 3	26	15	42	right prefrontal cortex (RPF)
Cls 4	-41	-16	44	left motor cortex (LM)
Cls 5	40	-19	44	right motor cortex (RM)
Cls 6	-17	-37	42	left parietal cortex (LP)
Cls 7	12	-41	39	right parietal cortex (RP)
Cls 8	12	-57	6	retrosplenial complex (RSC)
Cls 9	7	-87	24	occipital cortex (Occ)

843